J. Plasma Phys. (2024), *vol*. 90, 905900507
Published by Cambridge University Press

doi:10.1017/S0022377824001211

How Shock ignition can help to overcome the negative effects of hot electrons in direct-drive high-gain inertial confinement fusion

Mauro Temporal [1],‡, **Benoit Canaud** [2,3],† **and Rafael Ramis**[4]

[1]École Normale Supérieure Paris-Saclay, Centre Borelli UMR 9010, 4 avenue des Sciences, 91190 Gif sur Yvette, France

[2]CEA, DAM, DIF, F-91297 Arpajon, France

[3]Université Paris-Saclay, CEA, LMCE, 91680 Bruyères-le-Châtel, France

[4]ETSI Aeronáutica y del Espacio, Universidad Politécnica de Madrid, 28040 Madrid, Spain

(Received 13 May 2024; revised 27 August 2024; accepted 30 August 2024)

Hot electrons produced by parametric instabilities can negatively affect the thermonuclear gain of a direct-drive inertial confinement fusion capsule. A Monte Carlo transport is coupled to the hydrodynamics MULTI-IFE code in order to study the hot electron transport in a high-gain target implosion. The thermonuclear energy produced by the directly driven implosion of a reference target drops from 27 MJ without hot electrons to 13.5 kJ when the hot electrons are taken into account. A clear relationship is established between the level of hot electrons produced and the degradation of the thermonuclear yield produced by the target. It is shown that adding a relatively short laser spike (shock ignition) to the main pulse restores the thermonuclear energy released by the implosion. Different shock-ignition windows are presented depending on the duration of the spike. It appears that the longer the duration of the spike, the lower the power required for shock ignition. Finally, a 300 ps-duration spike requires only 50 TW to restore a thermonuclear energy output of 20 MJ.

Keywords: fusion plasma, plasma confinement

1. Introduction

Laser inertial confinement fusion (ICF) (Atzeni & Meyer-ter-Vehn 2004) uses the implosion of a spherical capsule to achieve the thermodynamic regime necessary to initiate and propagate a thermonuclear burning wave, which is able to release more fusion energy than energy invested in the implosion, producing what is commonly referred to as a high energy gain. Two main approaches are envisaged for the implosion of the target: direct drive (Craxton *et al.* 2015) and indirect drive (Lindl 1998). In the first case, the lasers

† Email address for correspondence: benoit.canaud@cea.fr
‡ Present address: Instituto de Investigaciones Energéticas (INEI), E.T.S.I.I., and CYTEMA, Universidad de Castilla-La Mancha, 13071 Ciudad Real, Spain.

directly illuminate the outer part of the spherical target while, in the indirect drive, the laser energy is converted into X-rays inside a cavity, usually of gold, and it is such X-rays that drive the implosion.

The capsule is a spherical envelope of low Z (plastic or CH) containing a layer of a mixture of deuterium (D) and tritium (T) in cryogenic form (at temperatures of approximately 19 K). The central part is filled with DT gas at saturation vapour pressure. The outer part consists of a layer, the ablator, that is vapourized by the lasers or the X-rays absorbed in it and transformed into plasma heated to very high temperatures (typically a few keV). This plasma, expelled at very high speed (a few hundred km.s^{-1}) from the outside of the target, exerts an inward radial pressure on the solid part of the target, which starts to move, imploding on itself until it collapses. The inner part, protected from lasers or X-rays, will be compressed and heated to very high temperatures, thus initiating fusion reactions and allowing the release of energy.

When lasers interact with the plasma, either in the cavity or directly on the target, so-called parametric instabilities (stimulated Raman scattering (Drake *et al.* 1974; Afeyan 1997*a*), and two plasmon decay (Figueroa *et al.* 1984; Afeyan 1997*b*)) are likely to produce very high energetic electrons – so-called supra-thermal or hot electrons – which have the particularity of penetrating deep into the capsule until they degrade the desired performance of the target (Temporal, Canaud & Ramis 2021*a*). This type of deleterious mechanism is much more significant in direct drive than in indirect drive, due to the fact that when the lasers strike the spherical target directly, the hot electron source is located much closer to the cryogenic DT. Parametric instabilities have multiple effects. Firstly, part of the laser power is involved in generating these instabilities near or below the critical quarter density, and is backscattered without being absorbed (Drake *et al*. 1974). This amount of laser energy is wasted and unused for ablation and shell velocity setting, thus impairing the laser–target coupling efficiency. Secondly, the hot electrons thus created can preheat the DT fuel (Christopherson *et al.* 2021), inducing a lowering of the shell density in the vicinity of the hot spot (Temporal *et al.* 2024) and thus increasing its adiabat. Thirdly, lowering the density and raising the temperature in this part of the target modifies the mean free path of the alphas, disrupting the release of thermonuclear energy (Temporal *et al.* 2024). All these effects, taken together, can prevent thermonuclear combustion, even if the hot-spot ignition conditions are fulfilled (Atzeni & Meyer-ter-Vehn 2004; Temporal *et al.* 2021*a*).

Various solutions (Dodd & Umstadter 2001; Wu *et al.* 2001; Albright, Yin & Afeyan 2014; Montgomery 2016; Zhou *et al.* 2018; Zhao *et al.* 2022) have been proposed to mitigate the detrimental effects of parametric instabilities, and thus, hot electrons, on the burning of a high-gain thermonuclear target. They are essentially all based on desynchronizing the laser coherence with respect to the electron plasma waves, by introducing a spectral width into the laser field, with many constraints on the laser installation.

Failing to eliminate parametric instabilities and their consequences in terms of hot electrons, it seems legitimate to consider the possibility of producing thermonuclear energy while generating hot electrons in the target due to parametric instabilities, by slightly modifying the thermodynamic conditions of the fuel at the moment of ignition. This is the aim of the work presented here. Hot electrons deposit their energy throughout the target, but their main effect is in the immediate vicinity of the hot spot, in the dense part of the shell (Temporal *et al.* 2024). The idea developed in the present work is to use a well-known ignition technique, shock ignition (SI) (Betti *et al.* 2007), to restore the target's thermonuclear energy gain. In fact, the aim here is to exploit shock ignition, not to demonstrate shock ignition of a target that does not ignite, but rather to use,

https://doi.org/10.1017/S0022377824001211 Published online by Cambridge University Press

simultaneously, the dual effect of using an ignition peak to both produce a non-isobaric situation conducive to easier ignition, but also to benefit from the increase, however slight, in implosion speed that the addition of the spike brings about, enabling the kinetic threshold of combustion to be shifted below the target's kinetic energy.

Shock ignition, first proposed by Betti *et al.* (2007), consists in igniting an ICF target in a non-isobaric way, where ignition is traditionally said to be isobaric or quasi-isobaric (Atzeni & Meyer-ter-Vehn 2004). The method used consists of adding a sub-nanosecond laser peak to the main pulse of an isentropic implosion, slightly modifying the latter to keep the peak implosion velocity constant. This method has met with real success, especially in numerical calculations, and many complementary studies have been carried out over the past two decades (Canaud & Temporal 2010; Schmitt *et al.* 2010; Atzeni *et al.* 2014), culminating in the use of this technique in the design of an inertial fusion reactor, the subject of the HiPER project (Dunne 2006; Ribeyre *et al.* 2008; Atzeni *et al.* 2009). Very quickly, the use of high laser powers, and therefore high intensities, led to the question of parametric instabilities and therefore of the hot electrons created by the ignition spike (Piriz *et al.* 2012). Some studies have demonstrated the benefits of energy transport in the ablator by these supra-thermal electrons (Klimo *et al.* 2014; Colaïtis *et al.* 2016; Cristoforetti *et al.* 2017; Llor Aisa *et al.* 2017; Trela *et al.* 2018). However, this is not the subject of the study presented here even if it is still a subject of actual research (Baton *et al.* 2020; Tentori *et al.* 2021; Barlow *et al.* 2022; Tentori, Colaïtis & Batani 2022*a*,*b*).

This work proposes to use shock ignition to overcome the deleterious effects of hot electrons on the performance of an ICF target. A baseline direct-drive ICF capsule implosion is considered and modelled by means of one-dimensional (1-D) numerical calculations using the Multi-IFE hydrodynamics code (Ramis & Meyer-ter-Vhen 2016). Hot electrons generated by parametric instabilities are transported through the target in which they deposit their energy with the consequence of significantly affecting the capsule's performance (Temporal *et al.* 2021*a*), although some electrons even appear to 'wander' (Gus'kov *et al.* 2019) in the target, which is likely to reduce their effect. A laser peak of a few hundred picoseconds is then added to the main laser pulse in order to ignite this non-igniting target.

The paper is organized as follows. Section 2 presents the baseline design consisting of the target and the laser pulse. Then, § 3 describes how the hot electrons and their transport in the target modify the implosion and the ignition of the capsule. Finally, the § 4 presents how the shock ignition allows restoration of the released thermonuclear energy and § 5 concludes the paper.

2. Baseline direct-drive target design

The target considered here (Temporal *et al.* 2021*a*, 2024; Temporal, Canaud & Ramis 2021*b*; Brandon *et al.* 2014) is a cryogenic spherical layer of thickness $\Delta = 198$ μm, inner radius $R_i = 593$ μm and total mass of 300 μg DT at the density of 0.25 g.cm^{-3}. The initial aspect ratio of the capsule $A = R_i/\Delta$ is 3. A plastic (CH) shell covers this cryogenic DT layer with a thickness of 30 μm for a density of 1.07 g.cm^{-3} and acts as a laser light absorber. The central part of the target is filled with DT gas at saturation vapour pressure (density 0.3 mg.cm^{-3}).

The capsule is directly irradiated by a laser pulse at wavelength $\lambda = 0.35$ μm (3ω) and laser light is assumed to propagate radially. Refraction is neglected and the absorption is calculated via inverse bremsstrahlung. A description of the capsule and the laser pulse are given in figure 1. The absorbed laser pulse is characterized by a low-power foot at the constant power of $P_1 = 0.6$ TW until the time t_1 followed by a Kidder-like ramp (Kidder 1976) such as $P(t) = P_0[1 - (t/\tau)^2]^a$ that grows until the time t_2 up to a maximum power

https://doi.org/10.1017/S0022377824001211 Published online by Cambridge University Press

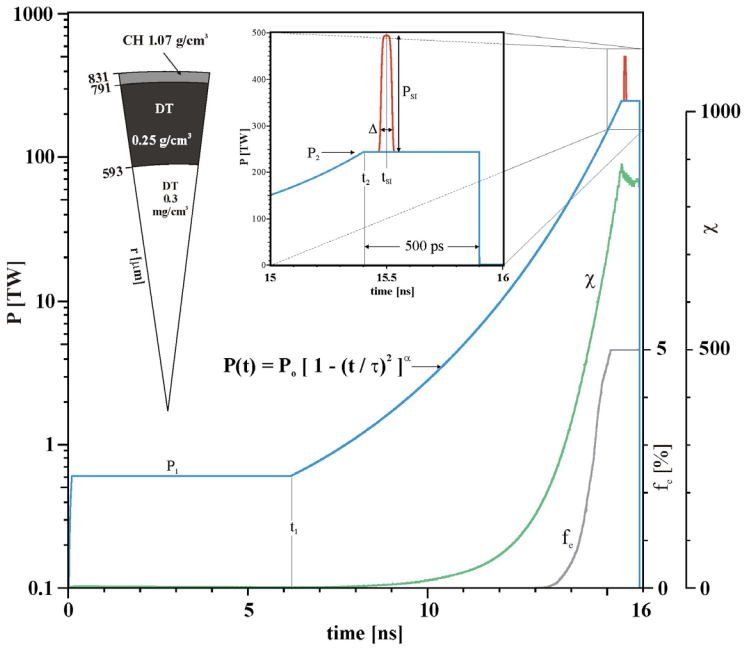

FIGURE 1. Sketch of the directly driven capsule and absorbed laser power as a function of time for the reference case (blue) and for the shock-ignition spike (red). Green (χ), grey (f_e) and dashed ($T_{\rm he}$) lines characterize hot electrons sources (see § 3).

P_2, of the drive, that stays constant for a relatively short drive of 500 ps. Thus the pulse depends on the four parameters t_1, t_2, P_2 and τ; whilst P_o and a are parameters calculated setting $P(t_1) = P_1$ and $P(t_2) = P_2$.

The 1-D hydrodynamics code Multi-IFE (Ramis & Meyer-ter-Vhen 2016) is used to optimize the parameters t_1, t_2, P_2 and τ. The MULTI code deals with multi-group radiation transport and tabulated equations of state, and ion and electron thermal conduction that assumes a harmonically limited (8 %) Spitzer heat flux (Spitzer 1962) at the free-flow limit.

The absorbed laser pulse (see blue curve in figure 1) results of a trade-off between minimizing the imploding kinetic energy (E_k) and minimizing the drive power and whole laser energy, while maximizing the thermonuclear output fusion energy (E_F). It is characterized by the parameters $t_1 = 6.2$ ns, $t_2 = 15.4$ ns, $\tau = 22.4$ ns and a top power drive of $P_2 = 242$ TW. Consequently, $P_o = 0.25$ TW and $\alpha = -10.7$. The corresponding absorbed energy is $E_a = 355$ kJ. For this reference case, the hydrodynamic calculation provides an output fusion energy of $E_F = 27.4$ MJ, a maximum kinetic energy of $E_k = 11.7$ kJ, a peak implosion velocity of $V = 251$ μm ns^{-1}, a stagnation time of $t_s = 16.09$ ns, a bang time (defined as the time of maximum fusion power) of $t_b = 16.19$ ns and an in-flight adiabat (defined as the ratio of DT pressure over Fermi pressure, taken during the deceleration phase) of $\alpha = P_{\rm DT}/P_{\rm Fermi} = P[\text{Mbar}]/2.32\rho^{5/3}[\text{g.cm}^{-3}] \sim 1.12$. The calculation related to this case, hereafter the reference case, neglects the production and transport of hot electrons and the loss of the power triggered by parametric instabilities.

We show in figure 1 an example of an ignition peak (in red) that can be considered. In all the calculations, the assumption will be made of an ignition peak in the form of

https://doi.org/10.1017/S0022377824001211 Published online by Cambridge University Press

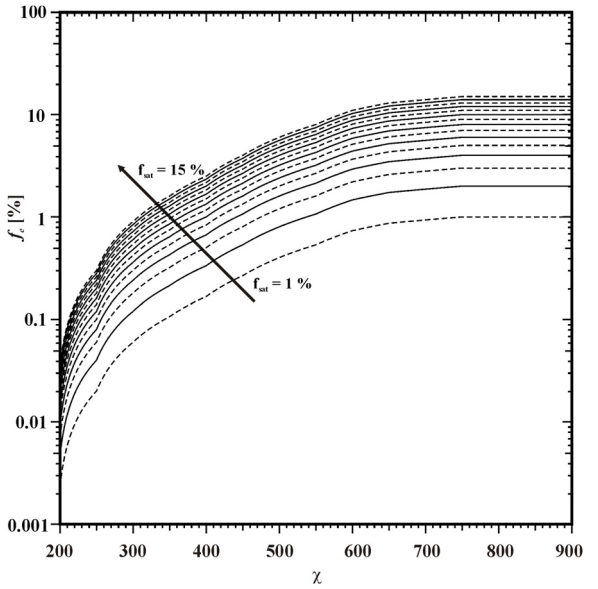

FIGURE 2. Hot-electron energy fraction ($f_{\rm he}$) evaluated for fifteen saturation values ($f_{\rm sat} = 1\,\%$ to $15\,\%$) as a function of the parameter χ.

a sixth-order super-Gaussian (quasi-square) temporal laser pulse centred at time $t_{\rm SI}$ with maximum power $P_{\rm SI}$ and full width at 1/*e*, Δ.

3. Hot electrons effects on burning target

A Monte Carlo package previously coupled to the Multi-IFE code for α-particles (Temporal *et al.* 2017) and fusion product transport (Temporal, Canaud & Ramis 2021*c*) has been adapted for the production, propagation and energy deposition of the hot electrons generated by plasma instabilities (Temporal *et al.* 2021*a*). In this package, the hot electrons are assumed to be generated at the radial position r_c of the quarter-critical plasma density, $n_c/4$, where n_c is the critical density. Following the work of Froula *et al.* (2012), the dimensionless parameter $\chi = IL_n/T_e$, normalized to 10^{14} (W.μm).(cm^2 keV)$^{-1}$, is used locally to estimate the temperature of the hot electrons $T_{\rm he}(\chi)$ as well as the fraction of the laser energy converted to hot electrons $f_e(\chi)$. Here, I, L_n and, T_e are the laser intensity, density gradient length and electron temperature, respectively, taken at the quarter-critical density.

In our study, the incoming laser intensity can be greater than 10^{15} W cm^{-2} while in Froula *et al.* (2012), laser intensity never exceeds this value. Anyway, in Solodov & Betti (2008), measurements have been done above 10^{15} W.cm^{-2}, showing the same trend as in Froula *et al.* (2012), namely saturation of the hot-electron fraction. The estimate of $T_{\rm he}$ is made using a numerical fit previously performed from the data of Froula *et al.* and more precisely from figure 4 in Froula *et al.* (2012), leading to $T_{\rm he}(\chi) = 100[\text{keV}]\chi/750$. Concerning f_e, a linear fit per part is made (Temporal *et al.* 2021*a*) from the experimental data presented in Froula *et al.* (2012). These data show a saturation of the hot-electron fraction f_e for χ larger than 750. The saturation level $f_{\rm sat}$ is used here as a free parameter. An example of χ and f_e is shown in figure 1 for the directly driven capsule without SI spike assuming a given saturation level ($f_{\rm sat} = 5\,\%$).

Figure 2 shows the variation of f_e with χ for ten $f_{\rm sat}$ saturation levels between 1 % and 15 %. The parameters χ, $T_{\rm he}$ and f_e are calculated at each hydrodynamic time step dt and

https://doi.org/10.1017/S0022377824001211 Published online by Cambridge University Press

used to create a population of electrons characterized by a Maxwellian distribution of temperature $T_{\rm he}$ and total energy $E_{\rm he} = f_e(\chi)P_L\,{\rm d}t$, where P_L is the absorbed laser power. The electron emission is assumed to be isotropic. During the hydrodynamic time step, the absorbed laser power is reduced by a factor $(1 - f_e)$ in order to ensure the conservation of the total energy. The hot electrons are assumed to move in a straight line over a distance Δs where 1 % of their energy is deposited, so that $\Delta s = 0.01 * \varepsilon/({\rm d}\varepsilon/{\rm d}s)$. The process proceeds step by step until the kinetic energy of the electrons is less than or equal to the temperature of the plasma.

In order to take into account the angular diffusion, at the end of each step Δs, the direction of the electrons is deflected by an angle θ and rotated by a random angle $\phi \in [0, 2\pi]$ around the incident direction Δs, where θ is the angle between the incident direction and the new direction and it follows a Gaussian distribution characterized by a standard deviation σ_θ (see (2) of Temporal *et al.* 2021*a*). The stopping power ${\rm d}\varepsilon/{\rm d}s$ (Atzeni, Schiavi & Davies 2008; Solodov & Betti 2008; Robinson *et al.* 2014) used to calculate the energy lost by the electrons as well as the calculation of σ_θ are detailed in Robinson *et al.* (2014) and Temporal *et al.* (2021*a*).

A series of calculations of a target implosion were performed using the 1-D Multi-IFE hydro-radiative code and varying the level of saturation ($f_{\rm sat}$) of hot-electron production between zero, corresponding to the reference case without hot electrons, and $f_{\rm sat} = 15\,\%$. It is worth noticing that the hot electrons and the induced laser power reduction have significant effects for low saturation levels (above 2 %) and lead to a strong reduction of the thermonuclear energy produced by the implosion.

The generation of parametric instabilities in the corona, accompanied by the creation of hot electrons, has two main consequences for implosion. The first concerns the energy deposition of these hot electrons as they propagate in the target, which will modify the hydrodynamics of the implosion and, in particular, the fuel adiabat. The second concerns the amount of laser energy absorbed by the plasma via inverse bremsstrahlung, which is reduced since some of it is either backscattered, in the case of stimulated Raman scattering, or converted directly into hot electrons, resulting in a reduction in laser–target coupling efficiency.

In order to identify the respective role of each consequence, two additional curves are presented in figure 3.

The first one (blue curve) concerns the reduction of the laser power due to the production of hot electrons without taking into account the energy deposition of the hot electrons. A second curve (green curve) concerns the energy deposition of hot electrons without taking into account the reduction of the laser power. This comparison shows that the transport and energy deposition of hot electrons inside the target have more important deleterious effects than the reduction of the absorbed laser power alone since the threshold is more or less the same when both effects are taken into account, whereas the threshold is 10 % when only the laser reduction is taken into account.

4. Shock ignition of baseline design with hot electrons

In a previous work (Temporal *et al.* 2021*a*), we have shown that the hot-electron energy deposition is more destructive the deeper it affects the target zones. It thus disturbs the hydrodynamic conditions of ignition and combustion of the gain target. The question is therefore whether shock ignition can be sufficiently effective in restoring the burning conditions of the DT. To verify this possibility, a representative case of marginal ignition (see figure 3, case a), corresponding to a saturation of $f_{\rm sat} = 5\,\%$ and producing only 13.5 kJ of thermonuclear energy, is considered. A series of calculations was performed by adding to the main laser pulse (blue curve in figure 1) a shock-ignition spike (red curve

https://doi.org/10.1017/S0022377824001211 Published online by Cambridge University Press

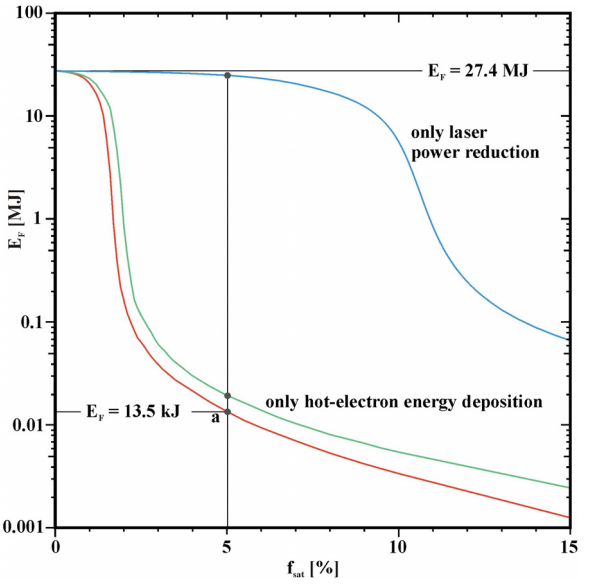

FIGURE 3. Thermonuclear output fusion energy E_F (MJ) as a function of the hot-electron saturation.

in figure 1), leading to an increase of the whole energy, characterized by a spike pulse centred at the time t_{SI}, a maximum spike power P_{SI} and six different spike time widths at $1/e$, $\Delta = 50$, 100, 200, 300, 400 and 500 ps. In these calculations, hot electrons are taken into account even for the spike with the same saturation level ($f_{sat} = 5\,\%$). The spike time t_{SI} ranges from 15.4 to 15.7 ns and the spike power ranges from 0 to 300 TW. The ignition window, defined as the thermonuclear fusion energy as a function of t_{SI} and P_{SI}, is shown in figure 4 for different spike widths. For all widths, there is a region in the parameter space that recovers combustion with thermonuclear energies above 20 MJ. Increasing the width Δ facilitates the ignition of the shock, with lower spike power P_{SI}.

The grey dots on the graphs of figure 4 show the positions of maximum thermonuclear energy in terms of spike power P_{SI} for each time t_{SI}. This is a ridgeline from which to follow the evolution of the thermonuclear energy for each peak power (deduced from the grey points).

It is worth noticing that the case $\Delta = 500$ ps is equivalent to increasing the power of the drive and thus the whole energy involved in the implosion. A series of calculations, carried out by varying the drive power above 242 TW, show that the thermonuclear energy of 27 MJ can be recovered again for an increase of the laser power of the drive of approximately 90 TW more, similarly to the case $\Delta = 500$ ps. Let us notice that, in this case ($\Delta = 500$ ps), the spike time is approximately 15.65 ns, which is equivalent to synchronizing the spike with the main drive.

Figure 5 shows the evolution of the thermonuclear energy as a function of the ridge power of the spike in the case of a full width at $1/e$ of $\Delta = 50$ ps (refers to the top left of figure 4).

At $P_{SI} = 0$ TW (without shock ignition), the implosion produces only 13.5 kJ of thermonuclear energy. By increasing the ridge power P_{SI}, the thermonuclear fusion energy increases and crosses a threshold that separates the marginally igniting implosions (for a low spike power) from burning implosions (for a sufficiently high spike power) tending asymptotically towards the 27.4 MJ of the reference case for the greatest spike power.

https://doi.org/10.1017/S0022377824001211 Published online by Cambridge University Press

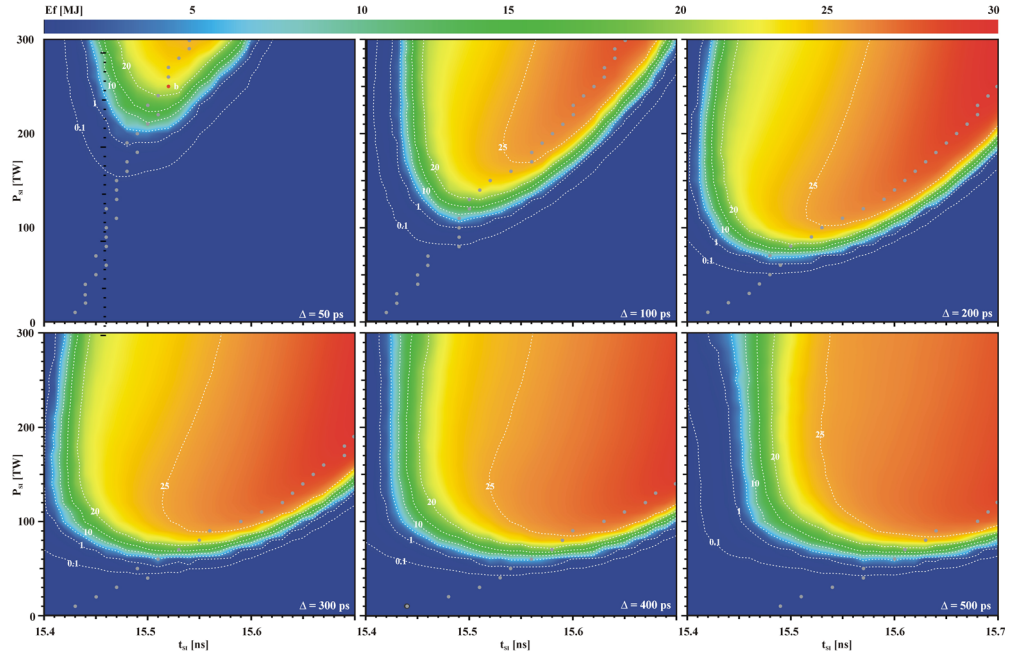

FIGURE 4. Thermonuclear fusion energy E_F (MJ) as a function of the spike parameters t_{SI} (ns) and P_{SI} (TW). The cases refer to a saturation level of $f_{sat} = 5\,\%$ and spike full width at $1/e$ $\Delta = 50$, 100, 200, 300, 400 and 500 ps.

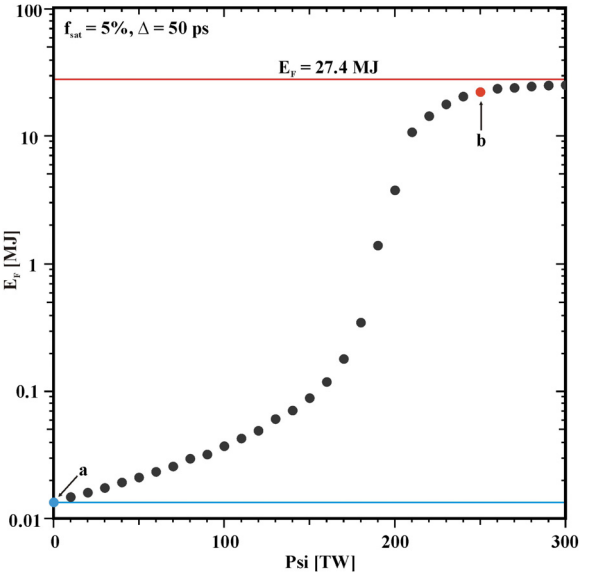

FIGURE 5. Maximum fusion energy as a function of the spike power P_{SI} for $\Delta = 50$ ps.

The threshold described here depends strongly on the duration of the spike, as shown in figure 6, where Δ varies from 50 to 500 ps, the last corresponding to the main pulse drive duration but not launched at the same time. The threshold is arbitrary defined as the smallest spike power for which the implosion of the target produces 1 MJ. The variation of this threshold is shown in figure 6 as a function of the spike duration Δ (red dots).

https://doi.org/10.1017/S0022377824001211 Published online by Cambridge University Press

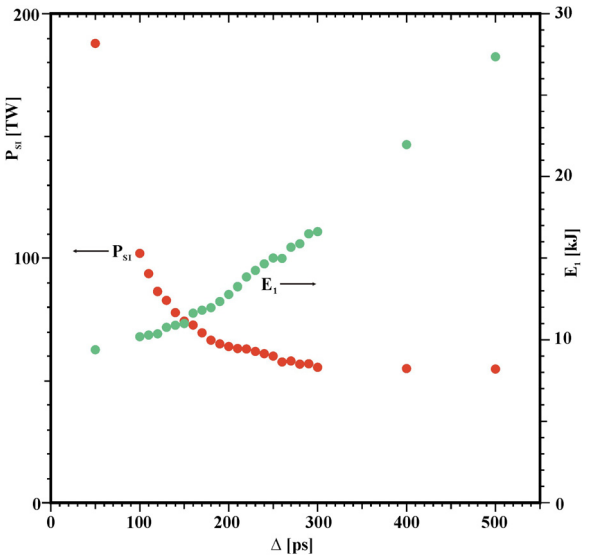

FIGURE 6. Minimum spike power (red dots) and absorbed laser energy (green dots) required for generating fusion energy of 1 MJ as a function of the spike duration Δ.

As shown earlier and inferred from figure 4, the minimum peak power required for producing at least 1 MJ decreases as the spike duration increases and almost saturates at approximately 55 TW for spike durations above 300 ps. For this last duration, the energy involved in ignition is roughly 15 kJ. This suggests that a minimal absorbed energy is required to initiate target combustion. The green curve in figure 6 represents the variation in the absorbed energy contained in the spike as a function of the duration of the peak Δ. This minimum energy to produce 1 MJ thermonuclear is here approximately 10 kJ for a spike duration of 50 ps.

Such a low level of spike power needed to ignite and burn an ICF target is not new and was already shown in Canaud & Temporal (2010), Canaud, Laffite & Temporal (2011), Temporal *et al.* (2011), Canaud *et al.* (2012) and Brandon *et al.* (2016). The novelty here is that, even when hot-electron energy deposition is taken into account, it is still possible to ignite the ICF target with relatively low spike power (below 200 TW). In addition, it is worth noticing that shorter spike duration requires lower spike energy (a spike of 50 ps requires only 9 kJ of additional energy against roughly 28 kJ for the spike of 500 ps).

In order to further investigate the hot-spot dynamics and following Brandon *et al.* (2016), we focus on the hot-spot thermodynamic paths of three distinct cases : the reference case, a case (*a*) without shock ignition and with hot electrons ($f_{\text{sat}} = 5\,\%$) and a case (*b*) with both hot electrons ($f_{\text{sat}} = 5\,\%$) and shock ignition with an ignition power $P_{\text{SI}} = 250$ TW (referred to as *b* in figures 4 and 5), $\Delta = 50$ ps and $t_{\text{SI}} = 15.52$ ns. In the first case (*a*), the fusion energy is $E_F = 13.5$ kJ while case (*b*) provides 21.3 MJ and gives back almost the 27.4 MJ of the baseline design. For all cases, the thermodynamic paths are evaluated in the (ρR_{HS}, T_{HS}) plane where $\rho R_{\text{HS}}(t)$ and $T_{\text{HS}}(t)$ are the time-resolved areal density and mass-averaged ionic temperature of the hot-spot volume, respectively. In this analysis, the Lagrangian cells where DT fusion occurs define the hot-spot volume. Figure 7 shows the hot-spot trajectories for the three cases during the deceleration phase (starting at the peak implosion velocity time) to stagnation (black dots, defined as the time of minimum volume for the hot spot) and then ignition or rebound without combustion.

https://doi.org/10.1017/S0022377824001211 Published online by Cambridge University Press

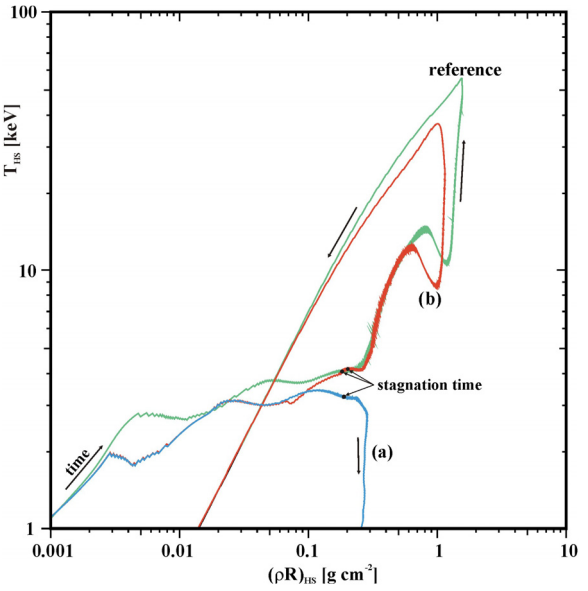

FIGURE 7. Temporal evolution of the hot-spot temperature T_{HS} and areal density ρR_{HS} for the reference case (green curve), the non-igniting case (*a*) and the shock-ignited case (*b*).

It can already be seen that the thermodynamic path of the reference case ('baseline' design) is clearly different from that of the target perturbed by the hot electrons (*a*), confirming that the hot electrons, in addition to disturbing the cryogenic DT (Christopherson *et al.* 2021; Temporal *et al.* 2021*a*), also manage to modify the thermodynamic path of the hot spot during the deceleration phase, while the laser is switched off. It can be seen that the temperature reached at stagnation by the perturbed target (*a*) is significantly lower (3 keV vs 4 keV) than that reached by the basic design while the hot-spot areal density is not modified. A simple shock is thus sufficient to close the 1 keV temperature gap and also recompress the dense shell to ignite and burn the target. Indeed, looking at the red curve corresponding to the thermodynamic path of the hot spot of the shock-ignited perturbed target, it is worth noting that the path follows that of the perturbed target up to a certain point and then deviates to follow that of the reference target. Following this end of the path to stagnation, the target ignites and burns almost like to the reference case, confirming that shock ignition overcomes the deleterious effects of hot electrons on a high-gain ICF target. Nevertheless, the maximum areal density of the shock-ignition case stands below the one from the reference case, leading to a lower thermonuclear energy.

5. Conclusions

This work shows the deleterious effects of hot electrons produced by parametric instabilities on the thermonuclear energy production of a high-gain target ($G \sim 77$) in direct-drive ICF and the possibility offered by shock ignition – obtained by adding a spike to the main pulse – to restore the high thermonuclear gain, initially lost by the effect of hot electrons. It is shown that a reference target producing approximately 27 MJ, only produces 13.5 kJ when the hot electrons and their transport in the target are taken into account.

https://doi.org/10.1017/S0022377824001211 Published online by Cambridge University Press

Different levels of saturation of the fraction of laser energy converted into hot electrons are considered using hydrodynamics simulations coupled with a Monte Carlo electron transport package. A direct relationship is established between the level of hot electrons produced and the degradation of the thermonuclear yield. Finally, adding a laser spike to the main pulse restores the thermonuclear energy released by the implosion. Different shock-ignition windows are presented depending on the duration of the spike. It clearly appears that, the longer the duration of the spike, the lower the power required for shock ignition.

A spike power threshold appears, defined as the power required to produce 1 MJ of thermonuclear energy. The threshold on spike power decreases with the duration of the spike until a spike duration of 300 ps when the threshold power saturates around 50 TW. For a spike duration of 300 ps, the energy contained in the spike is very low, around 15 kJ, for a power of around 50 TW.

It is also necessary to put these results into perspective with regard to the method used. Indeed, in the calculations, the laser propagates radially, and its absorption takes place at greater depth than in a situation where a focal spot would be taken into account. As such, the results presented here should be considered more qualitatively than quantitatively.

Acknowledgements

Editor Louise Willingale thanks the referees for their advice in evaluating this paper.

Funding

M.T. has been supported by the CEA-ENS LRC-MESO grant no2018-011. R.R. has been supported by the Spanish *Ministerio de Ciencia Innovacion y Universidades* project RTI2018-098801-B-100.

Declaration of interests

The authors report no conflict of interest.

REFERENCES

AFEYAN, B.B. 1997*a* A variational approach to parametric instabilities in inhomogeneous plasmas II: stimulated Raman scattering. *Phys. Plasmas* **22** (4), 3803.

AFEYAN, B.B. 1997*b* A variational approach to parametric instabilities in inhomogeneous plasmas III: two-plasmon decay. *Phys. Plasmas* **22** (4), 3827.

ALBRIGHT, J., YIN, L. & AFEYAN, B. 2014 Control of stimulated Raman scattering in the strongly nonlinear and kinetic regime using spike trains of uneven duration and delay. *Phys. Rev. Lett*. **113**, 045002.

ATZENI, S., DAVIES, J.R., HALLO, L., HONRUBIA, J.J., MAIRE, P.H., OLAZABAL-LOUMÉ, M., FEUGEAS, J.L., RIBEYRE, X., SCHIAVI, A., SCHURTZ, G., BREIL, J. & NICOLAÏ, P. 2009 Studies on targets for inertial fusion ignition demonstration at the HiPER facility. *Nucl. Fusion* **49**, 055008.

ATZENI, S. & MEYER-TER-VHEN, J. 2004 *The Physics of Inertial Fusion*. Oxford Science Press.

ATZENI, S., RIBEYRE, X., SCHURTZ, G., SCHMITT, A.J., CANAUD, B., BETTI, R. & PERKINS, L.J. 2014 Shock ignition of thermonuclear fuel: principles and modelling. *Nucl. Fusion* **54**, 054008.

ATZENI, S., SCHIAVI, A. & DAVIES, J.R. 2008 Stopping and scattering of relativistic electron beams in dense plasmas and requirements for fast ignition. *Plasma Phys. Control. Fusion* **51**, 015016.

BARLOW, D., GOFFREY, T., BENNETT, K., SCOTT, R.H.H., GLIZE, K., THEOBALD, W., ANDERSON, K., SOLODOV, A.A., ROSENBERG, M.J., WOOLSEY, N.C., BRADFORD, P., KHAN, M. & ARBER, T.D. 2022 Role of hot electrons in shock ignition constrained by experiment at the National Ignition Facility. *Phys. Plasmas* **29**, 082704.

Baton, S.D., *et al*. 2020 Preliminary results from the LMJ-PETAL experiment on hot electrons characterization in the context of shock ignition. *High Energy Density Phys*. **36**, 100796.

Betti, R., Zhou, C.D., Anderson, K.S., Perkins, L.J., Theobald, W. & Solodov, A.A. 2007 Shock ignition of thermonuclear fuel with high areal density. *Phys. Rev. Lett*. **98**, 155001.

Brandon, V., Canaud, B., Temporal, M. & Ramis, R. 2014 Low initial aspect-ratio direct-drive target designs for shock-or self-ignition in the context of the laser Megajoule. *Nucl. Fusion* **54**, 083016.

Brandon, V., Canaud, B., Temporal, M. & Ramis, R. 2016 Thermodynamic properties of thermonuclear fuel in inertial confinement fusion. *Laser Part. Beams* **34**, 539.

Canaud, B., Laffite, S., Brandon, V. & Temporal, M. 2012 2D analysis of direct-drive shock-ignited HiPER-like target implosions with the full laser megajoule. *Laser Part. Beams* **30**, 183.

Canaud, B., Laffite, S. & Temporal, M. 2011 Shock ignition of direct-drive double-shell targets. *Nucl. Fusion* **51**, 062001.

Canaud, B. & Temporal, M. 2010 High-gain shock ignition of direct-drive ICF targets for the Laser Mégajoule. *New J. Phys*. **12**, 043037.

Christopherson, A.R., *et al*. 2021 Direct measurements of DT fuel preheat from hot electrons in direct-drive inertial confinement fusion. *Phys. Rev. Lett*. **127**, 055001.

Colaïtis, A., Ribeyre, X., Le Bel, E., Duchateau, G., Nicolaï, P. & Tikhonchuk, V. 2016 Influence of laser induced hot electrons on the threshold for shock ignition of fusion reactions. *Phys. Plasmas* **23**, 072703.

Craxton, R.S., *et al*. 2015 Direct-drive inertial confinement fusion: a review. *Phys. Plasmas* **22**, 110501.

Cristoforetti, G., Colaïtis, A., Antonelli, L., Atzeni, S., Baffigi, F., Batani, D., Barbato, G., Dudzak, R., Koester, P., Krousky, E., Labate, L., Nicolaï, P., Renner, O., Skoric, M., Tikhonchuk, V. & Gizzi, L.A. 2017 Experimental observation of parametric instabilities at laser intensities relevant for shock ignition. *Eur. Phys. Lett*. **117**, 35001.

Dodd, E.S. & Umstadter, D. 2001 Coherent control of stimulated Raman scattering using chirped laser pulses. *Phys. Plasmas* **8**, 3531.

Drake, J.F., Kaw, P.K., Lee, Y.C., Schmid, G., Liu, C.S. & Rosenbluth, M.N. 1974 Parametric instabilities of electromagnetic waves in plasmas. *Phys. Fluids* **17**, 778.

Dunne, M. 2006 A high-power laser fusion facility for Europe. *Nat. Phys*. **2**, 2.

Figueroa, H., Joshi, C., Azechi, H., Ebrahim, N.A. & Estabrook, K. 1984 Stimulated Raman scattering, two-plasmon decay, and hot electron generation from underdense plasmas at 0.35 μm. *Phys. Fluids* **27**, 1887.

Froula, D.H., Yaakobi, B., Hu, S.X., Chang, P.Y., Craxton, R.S., Edgell, D.H., Follett, R., Michel, D.T., Myatt, J.F., Seka, W., Short, R.W., Solodov, A. & Stoeckl, C. 2012 Saturation of the two-plasmon decay instability in long-scale-length plasmas relevant to direct-drive inertial confinement fusion. *Phys. Rev. Lett*. **108**, 165003.

Gus'kov, S.Y., Kuchugov, P.A., Yakhin, R.A. & Zmitrenko, N.V. 2019 Effect of fast electrons on the gain of a direct-drive laser fusion target. *Plasma Phys. Control. Fusion* **61**, 105014.

Kidder, R.E. 1976 Energy gain of laser-compressed pellets: a simple model calculation. *Nucl. Fusion* **16**, 405.

Klimo, O., Psikal, J., Tikhonchuk, V.T. & Weber, S. 2014 Two-dimensional simulations of laser–plasma interaction and hot electron generation in the context of shock-ignition research. *Plasma Phys. Control. Fusion* **56**, 055010.

Lindl, J.D. 1998 *Inertial Confinement Fusion: The Quest for Ignition and high Gain using Indirect Drive*. Springer.

Llor Aisa, E., Ribeyre, X., Duchateau, G., Nguyen-Bui, T., Tikhonchuk, V.T., Colaïtis, A., Betti, R., Bose, A. & Theobald, W. 2017 The role of hot electrons in the dynamics of a laser-driven strong converging shock. *Phys. Plasmas* **24**, 112711.

Montgomery, D.S. 2016 Two decades of progress in understanding and control of laser plasma instabilities in indirect drive inertial fusion. *Phys. Plasmas* **23**, 055601.

PIRIZ, A.R., RODRIGUEZ PRIETO, G., TAHIR, N.A., ZHANG, Y., LIU, S.D. & ZHAO, Y.T. 2012 Ablation driven by hot electrons generated during the ignitor laser pulse in shock ignition. *Phys. Plasmas* **19**, 122705.

RAMIS, R. & MEYER-TER-VEHN, J. 2016 Multi-IFE—a one-dimensional computer code for Inertial Fusion Energy (IFE) target simulations. *Comput. Phys. Commun*. **203**, 226.

RIBEYRE, X., SCHURTZ, G., LAFON, M., GALERA, S. & WEBER, S. 2008 Shock ignition: an alternative scheme for HiPER. *Plasma Phys. Control. Fusion* **51**, 015013.

ROBINSON, A.P.L., STROZZI, D.J., DAVIES, J.R., GREMILLET, L., HONRUBIA, J.J., JOHZAKI, T., KINGHAM, R.J., SHERLOCK, M. & SOLODOV, A.A. 2014 Theory of fast electron transport for fast ignition. *Nucl. Fusion* **54**, 054003.

SCHMITT, A.J., BATES, J.W., OBENSCHAIN, S.P., ZALESAK, S.T. & FYFE, D.E. 2010 Shock ignition target design for inertial fusion energy. *Phys. Plasmas* **17**, 042701.

SOLODOV, A.A. & BETTI, R. 2008 Stopping power and range of energetic electrons in dense plasmas of fast-ignition fusion targets. *Phys. Plasmas* **15**, 042707.

SPITZER, L. 1962 *Physics of Fully Ionized Plasmas*. Wiley Inter-science.

TEMPORAL, M., CANAUD, B., CAYZAC, W., RAMIS, R. & SINGLETON, R.L. 2017 Effects of alpha stopping power modelling on the ignition threshold in a directly-driven inertial confinement fusion capsule. *Eur. Phys. J.* D **71**, 132.

TEMPORAL, M., CANAUD, B. & RAMIS, R. 2021*a* Effect of hot-electron distribution in the thermonuclear burn degradation in Directly-Driven Inertial Confinement Fusion. *Eur. Phys. J.* D **75**, 300.

TEMPORAL, M., CANAUD, B. & RAMIS, R. 2021*b* Dependence of Inertial Confinement Fusion capsule performance on fuel reaction rate. *Eur. Phys. J.* D **75**, 8.

TEMPORAL, M., CANAUD, B. & RAMIS, R. 2021*c* Direct-drive target designs as energetic particle sources for the Laser MégaJoule facility. *J. Plasma Phys*. **87**, 905870208.

TEMPORAL, M., PIRIZ, A.R., CANAUD, B. & RAMIS, R. 2024 Alpha particles range modified by hot electrons adversely affects the energy threshold in direct-drive inertial confinement fusion. *Eur. Phys. J. Plus* **139**, 2.

TEMPORAL, M., RAMIS, R., CANAUD, B., BRANDON, V., LAFFITE, S. & LE GARREC, B.J. 2011 Irradiation uniformity of directly driven inertial confinement fusion targets in the context of the shock-ignition scheme. *Plasma Phys. Control. Fusion* **53**, 124008.

TENTORI, A., COLAÏTIS, A. & BATANI, D. 2022*a* 3D Monte-Carlo model to study the transport of hot electrons in the context of inertial confinement fusion. Part I. *Matt. Rad. Ext*. **7**, 065902.

TENTORI, A., COLAÏTIS, A. & BATANI, D. 2022*b* 3D Monte-Carlo model to study the transport of hot electrons in the context of inertial confinement fusion. Part II. *Matt. Rad. Ext*. **7**, 065903.

TENTORI, A., COLAÏTIS, A., THEOBALD, W., CASNER, A., RAFFESTIN, D., RUOCCO, A., TRELA, J., LE BEL, E., ANDERSON, K., WEI, M., HENDERSON, B., PEEBLES, J., SCOTT, R., BATON, S., PIKUZ, S.A., BETTI, R., KHAN, M., WOOLSEY, N., ZHANG, S. & BATANI, D. 2021 Experimental characterization of hot-electron emission and shock dynamics in the context of the shock ignition approach to inertial confinement fusion. *Phys. Plasmas* **28**, 103302.

TRELA, J., THEOBALD, W., ANDERSON, K.S., BATANI, D., BETTI, R., CASNER, A., DELETTREZ, J.A., FRENJE, J.A., GLEBOV, V.Y., RIBEYRE, X., SOLODOV, A.A., STOECKL, M. & STOECKL, C. 2018 The control of hot-electron preheat in shock-ignition implosions. *Phys. Plasmas* **25**, 052707.

WU, Y.Q., HAN, S.S., SONG, X.Y., XU, Z.Z., TANG, Y.H. & SHUAI, B. 2001 The control of laser-plasma parametric instabilities and the temperature of suprathermal electrons with ultrabroad bandwidth frequency modulated laser pulse. *Plasma Phys. Control. Fusion* **43**, 469.

ZHAO, Y., WENG, S.M., MA, H.H., BAI, X.J. & SHENG, Z.M. 2022 Mitigation of laser plasma parametric instabilities with broadband lasers. *Rev. Mod. Plasma Phys*. **7**, 1.

ZHOU, H.Y., XIAO, C.Z., ZOU, D.B., LI, X.Z., YIN, Y., SHAO, F.Q. & ZHUO, H.B. 2018 Numerical study of bandwidth effect on stimulated Raman backscattering in nonlinear regime. *Phys. Plasmas* **25**, 062703.

https://doi.org/10.1017/S0022377824001211 Published online by Cambridge University Press